

# Gamma-ray Constraints on Effective Interactions of the Dark Matter

Kingman Cheung<sup>1,2</sup>, Po-Yan Tseng<sup>2</sup> and Tzu-Chiang Yuan<sup>3</sup>

<sup>1</sup>*Division of Quantum Phases & Devices, School of Physics,  
Konkuk University, Seoul 143-701, Korea*

<sup>2</sup>*Department of Physics, National Tsing Hua University, Hsinchu 300, Taiwan*

<sup>3</sup>*Institute of Physics, Academia Sinica, Nankang, Taipei 11529, Taiwan*

(Dated: March 7, 2019)

## Abstract

Using an effective interaction approach to describe the interactions between the dark matter particle and the light degrees of freedom of the standard model, we calculate the gamma-ray flux due to the annihilation of the dark matter into quarks, followed by fragmentation into neutral pions which subsequently decay into photons. By comparison to the mid-latitude data released from the Fermi-LAT experiment, we obtain useful constraints on the size of the effective interactions and they are found to be comparable to those deduced from collider, gamma-ray line and anti-matter search experiments. However, the two operators induced by scalar and vector exchange among fermionic dark matter and light quarks that contribute to spin-independent cross sections are constrained more stringently by the recent XENON100 data.

## I. INTRODUCTION

The presence of cold dark matter (CDM) in our Universe is now well established by a number of observational experiments, especially the very precise measurement of the cosmic microwave background radiation in the Wilkinson Microwave Anisotropy Probe (WMAP) experiment [1]. The measured value of the CDM relic density is

$$\Omega_{\text{CDM}} h^2 = 0.1126 \pm 0.0036 , \quad (1)$$

where  $h$  is the Hubble constant in units of 100 km/Mpc/s. Though the gravitation nature of the dark matter is commonly believed to be well established, its particle nature remains allure except that it is nonbaryonic and to a high extent electrically neutral.

One of the most appealing and natural CDM particle candidates is the *weakly-interacting massive particle* (WIMP). It is a coincidence that if the dark matter (DM)  $\chi$  is thermally produced in the early Universe, the required annihilation cross section is right at the order of weak interaction. The relation between the fractional relic density of  $\chi$  relative to the critical density and its thermal annihilation cross section can be given by the following simple formula [2]

$$\Omega_{\chi} h^2 \simeq \frac{0.1 \text{ pb}}{\langle \sigma v \rangle} , \quad (2)$$

with  $\langle \sigma v \rangle$  being the annihilation cross section of the dark matter around the time of freeze-out, at which the annihilation rate could no longer catch up with the Hubble expansion rate of the Universe. Assuming the measured  $\Omega_{\text{CDM}} h^2$  to be saturated by a single component WIMP, its annihilation cross section should be about 1 pb or  $3 \times 10^{-26} \text{ cm}^3 \text{ s}^{-1}$ . This is exactly the size of the cross section that one expects from a weak interaction process, which implies an appreciable size of production rate of the WIMP at the Large Hadron Collider (LHC) as well as the event rates for direct and indirect searches that reach the sensitivities of dark matter experiments like XENON100 and Fermi-LAT respectively. In general, production of dark matter at the LHC would give rise to a large missing energy. Thus, the anticipated signature in the final state is high- $p_T$  jets or leptons plus a large missing energy. Note that there could be non-thermal sources for the dark matter, such as decay from exotic relics like moduli fields, cosmic strings, etc. In such cases, the annihilation cross section in Eq. (2) can be larger than the value quoted above.

There have been many proposed candidates for the dark matter. Without committing

to any particular DM model so as to perform a model independent analysis, we adopt an effective interaction approach to describe the interactions of the dark matter particle with the standard model (SM) particles [3–15]. One simple realization of the effective interaction approach is that the dark matter particle exists in a hidden sector, which communicates to the SM sector via a heavy degree of freedom in the connector sector. At energy scale well below this heavy mediator the interactions can be conveniently described by a set of effective interactions. The strength of each interaction depends on the nature of the dark matter particle and the mediator. The most important set of interactions are among the fermionic dark matter  $\chi$  and the light quarks  $q$  described by the effective operators  $(\bar{\chi}\Gamma\chi)(\bar{q}\Gamma'q)$  where  $\Gamma$  and  $\Gamma'$  are general Dirac matrices contracted with appropriate Lorentz indices. We will discuss these and other operators in more details in the next section.

There have been some recent works on constraining the interactions at present and future collider experiments [3–6], using gamma-ray experiments [7–10] and using anti-matter search experiments [13–15]. There was another work in which the dark matter couples only to the top quark and corresponding predictions at direct and indirect detection experiments as well as colliders were obtained [12]. It was also shown in Ref. [16] that additional radiation of electroweak bosons in the final state can modify the energy spectrum, especially at the lower end of the spectrum. Lifting the helicity suppression by radiating off an electroweak gauge boson from the external light fermion legs due to Majorana dark matter annihilation is emphasized in Ref. [16, 17].

In Ref. [8], monochromatic photon-line flux was calculated via a loop with quarks running in it and photons being attached to the internal quark line. Although the photon-line would be a smoking-gun signal to compare with the data, the rate is suppressed because of the loop factor. On the other hand, photons can come from the decay of neutral pions, which in turn come from the fragmentation of the quarks in the annihilation of the dark matter. The chance that an energetic quark fragments into neutral pions is high and the branching ratio of a neutral pion into two photons is 98.823% [18]. Therefore, the amount of photons coming from the quark fragmentation is much larger than those coming off a loop process. Nevertheless, the spectrum of such photons is continuous and in general have no structure, except for a cutoff due to the mass of the dark matter. In this work, we focus on the continuous gamma-ray flux spectrum coming from the fragmentation of quarks into neutral pions, followed by their decays into photons, in the annihilation of the dark matter. Such

annihilation of the dark matter will give rise to an additional source of diffuse gamma-rays other than the known backgrounds. If the experimental measurement is consistent with the known gamma-ray background estimation, then one could use the data to constrain the amount of gamma-ray flux coming from the dark matter annihilation, thus constraining the effective interactions between the dark matter and the quarks.

The data on the photon spectrum from the mid-latitude ( $10^\circ < |b| < 20^\circ$ ,  $0^\circ < l < 360^\circ$ ) [19] recorded by the Fermi-LAT indicated a continuous spectrum and mostly consistent with the known backgrounds. We can therefore use the data to constrain on additional sources of gamma-ray, namely, the annihilation of the dark matter into quarks, followed by fragmentation into neutral pions, which further decay into photons. The production of photons via neutral pions is the dominant mechanism for gamma-rays. There are also other ways that the quarks from annihilation of dark matter can produce gamma rays, such as bremsstrahlung off quark legs, synchrotron radiation, or inverse Compton scattering on background photons, but these processes are all  $\alpha_{\text{em}}$  suppressed relative to the fragmentation of the quarks into neutral pions. We focus on the fragmentation of the quarks coming from the annihilation of the dark matter as the signal in our analysis. We employ two approaches of obtaining the photon spectrum due to fragmentation of light quarks. (i) We use the process  $e^+e^- \rightarrow q\bar{q}$  with initial radiations turned off in Pythia [20] and extract the photon spectrum in the final state. The photon mainly comes from the decay of  $\pi^0$ , which are in turn produced by fragmentation of light quarks, plus a very small fraction from the bremsstrahlung photon off the quark legs. (ii) We use the fragmentation function of  $q, \bar{q}, g$  into  $\pi^0$  from the fitting of Ref. [21], then convolute with the  $dN/dE_\gamma(\pi^0 \rightarrow \gamma\gamma)$  to obtain the photon spectrum of quarks into photon. We found that both approaches give almost the same photon spectrum from light quarks. The resulting limits using both approaches are also the same within numerical accuracy. However, we have to use the second approach when we place limits on the operators involving gluons, because we do not find an appropriate process in Pythia for extraction of  $g \rightarrow \gamma$  fragmentation.

The choice of the mid-latitude data instead of the Galactic Center is simply because the gamma-ray in this region is dominated by local sources and we have clarity in understanding the background flux and point sources within the mid-latitude. On the other hand, the Galactic center is supposed to have a number of known and known-unknown point sources, including a supermassive black hole near the Center, and perhaps some unknown sources too.

Given the purpose of constraining the new DM interactions it is better to understand clearly about the background in mid-latitude, rather than the larger flux from the Galactic Center. The Galactic diffuse gamma rays originate primarily from the interactions of high energy charged particles contained in cosmic rays with the nuclei in the interstellar medium and the associated radiation fields of the charged particles, via a few mechanisms briefly described in Sec. III. While most of them are well understood, the extra-galactic component has a larger uncertainty. We will choose a normalization such that the total background diffuse gamma-ray flux is consistent with the Fermi-LAT measurement of diffuse gamma-ray flux in the mid-latitude. This approach is the same as the Fermi-LAT when they estimated the extra-galactic diffuse component [19].

The organization of the paper is as follows. In the next section, we describe the interactions between the dark matter particle and the SM particles, in particular quarks and gluons. In Sec. III, we discuss various sources of diffuse gamma-ray flux that constitute the known background and calculate the gamma-ray flux due to the dark matter annihilation using the effective interactions. We compare with other constraints and conclude in Sec. IV.

## II. EFFECTIVE INTERACTIONS

For simplicity, we will assume there is only one component of dark matter denoted by  $\chi$  and it is a standard model singlet.

The first set of operators we will be considering is for fermionic DM and its effective interactions with light quarks via a (axial) vector- or tensor-type exchange are given by the following dimension 6 operators

$$\mathcal{L}_{i=1-6} = \frac{C}{\Lambda_i^2} (\bar{\chi}\Gamma\chi) (\bar{q}\Gamma'q) , \quad (3)$$

where  $\Gamma, \Gamma' = \gamma^\mu, \gamma^\mu\gamma^5, \sigma^{\mu\nu}$  or  $\sigma^{\mu\nu}\gamma^5$  with  $\sigma^{\mu\nu} \equiv i(\gamma^\mu\gamma^\nu - \gamma^\nu\gamma^\mu)/2$ .  $\Lambda_i$  is the heavy scale for the connector sector that has been integrated out and  $C$  is an effective coupling constant of order  $O(1)$ . It is understood that for Majorana fermion the vector and tensor structures of  $\Gamma$  are absent. Thus, for vector or tensor type interaction the fermion  $\chi$  in Eq.(3) is understood to be Dirac. We will be focusing on Dirac fermionic DM in this work, but our results are also applicable to Majorana dark matter. Note also that due to the following identity

$$\sigma^{\mu\nu}\gamma^5 = \frac{i}{2}\epsilon^{\mu\nu\alpha\beta}\sigma_{\alpha\beta} , \quad (4)$$

TABLE I. The list of effective interactions between the dark matter and the light degrees of freedom (quark or gluon). We have suppressed the color index on the quark and gluon fields. These operators have also been analyzed in Refs. [3, 5, 8, 13].

Operator	Coefficient	Velocity Scaling in $\langle\sigma v\rangle$
Dirac DM, (axial) vector/tensor exchange		
$O_1 = (\bar{\chi}\gamma^\mu\chi)(\bar{q}\gamma_\mu q)$	$\frac{C}{\Lambda^2}$	$m_\chi^2$
$O_2 = (\bar{\chi}\gamma^\mu\gamma^5\chi)(\bar{q}\gamma_\mu q)$	$\frac{C}{\Lambda^2}$	$m_\chi^2 v^2$
$O_3 = (\bar{\chi}\gamma^\mu\chi)(\bar{q}\gamma_\mu\gamma^5 q)$	$\frac{C}{\Lambda^2}$	$m_\chi^2$
$O_4 = (\bar{\chi}\gamma^\mu\gamma^5\chi)(\bar{q}\gamma_\mu\gamma^5 q)$	$\frac{C}{\Lambda^2}$	$m_\chi^2 v^2$
$O_5 = (\bar{\chi}\sigma^{\mu\nu}\chi)(\bar{q}\sigma_{\mu\nu} q)$	$\frac{C}{\Lambda^2}$	$m_\chi^2$
$O_6 = (\bar{\chi}\sigma^{\mu\nu}\gamma^5\chi)(\bar{q}\sigma_{\mu\nu} q)$	$\frac{C}{\Lambda^2}$	$m_\chi^2$
Dirac DM, (pseudo) scalar exchange		
$O_7 = (\bar{\chi}\chi)(\bar{q}q)$	$\frac{Cm_q}{\Lambda^3}$	$m_q^2 m_\chi^2 v^2$
$O_8 = (\bar{\chi}\gamma^5\chi)(\bar{q}q)$	$\frac{iCm_q}{\Lambda^3}$	$m_q^2 m_\chi^2$
$O_9 = (\bar{\chi}\chi)(\bar{q}\gamma^5 q)$	$\frac{iCm_q}{\Lambda^3}$	$m_q^2 m_\chi^2 v^2$
$O_{10} = (\bar{\chi}\gamma^5\chi)(\bar{q}\gamma^5 q)$	$\frac{Cm_q}{\Lambda^3}$	$m_q^2 m_\chi^2$
Dirac DM, gluonic		
$O_{11} = (\bar{\chi}\chi)G_{\mu\nu}G^{\mu\nu}$	$\frac{C\alpha_s}{4\Lambda^3}$	$m_\chi^4 v^2$
$O_{12} = (\bar{\chi}\gamma^5\chi)G_{\mu\nu}G^{\mu\nu}$	$\frac{iC\alpha_s}{4\Lambda^3}$	$m_\chi^4$
$O_{13} = (\bar{\chi}\chi)G_{\mu\nu}\tilde{G}^{\mu\nu}$	$\frac{C\alpha_s}{4\Lambda^3}$	$m_\chi^4 v^2$
$O_{14} = (\bar{\chi}\gamma^5\chi)G_{\mu\nu}\tilde{G}^{\mu\nu}$	$\frac{iC\alpha_s}{4\Lambda^3}$	$m_\chi^4$
Complex Scalar DM, (axial) vector exchange		
$O_{15} = (\chi^\dagger\overleftrightarrow{\partial}_\mu\chi)(\bar{q}\gamma^\mu q)$	$\frac{C}{\Lambda^2}$	$m_\chi^2 v^2$
$O_{16} = (\chi^\dagger\overleftrightarrow{\partial}_\mu\chi)(\bar{q}\gamma^\mu\gamma^5 q)$	$\frac{C}{\Lambda^2}$	$m_\chi^2 v^2$
Complex Scalar DM, (pseudo) scalar exchange		
$O_{17} = (\chi^\dagger\chi)(\bar{q}q)$	$\frac{Cm_q}{\Lambda^2}$	$m_q^2$
$O_{18} = (\chi^\dagger\chi)(\bar{q}\gamma^5 q)$	$\frac{iCm_q}{\Lambda^2}$	$m_q^2$
Complex Scalar DM, gluonic		
$O_{19} = (\chi^\dagger\chi)G_{\mu\nu}G^{\mu\nu}$	$\frac{C\alpha_s}{4\Lambda^2}$	$m_\chi^2$
$O_{20} = (\chi^\dagger\chi)G_{\mu\nu}\tilde{G}^{\mu\nu}$	$\frac{iC\alpha_s}{4\Lambda^2}$	$m_\chi^2$

the axial tensor  $\sigma^{\mu\nu}\gamma^5$  is related to the tensor  $\sigma^{\alpha\beta}$  and thus should not be regarded as an independent set for Dirac fermionic DM. However, for Majorana fermionic  $\chi$ , such axial tensor structure can be present.

Next set of operators are associated with (pseudo) scalar-type exchange

$$\mathcal{L}_{i=7-10} = \frac{Cm_q}{\Lambda_i^3} (\bar{\chi}\Gamma\chi) (\bar{q}\Gamma'q) , \quad (5)$$

where  $\Gamma, \Gamma' = 1$  or  $i\gamma^5$ . The  $m_q$  dependence in the coupling strength is included for scalar-type interactions in accord with the trace anomaly in QCD. We use the current quark masses in the Lagrangian given by [18]:

$$\begin{aligned} m_u &= 0.0025 \text{ GeV}, & m_d &= 0.005 \text{ GeV}, & m_s &= 0.101 \text{ GeV}, \\ m_c &= 1.27 \text{ GeV}, & m_b &= 4.19 \text{ GeV}, & m_t &= 172 \text{ GeV}. \end{aligned}$$

Another light degree of freedom that couples to the Dirac dark matter is the gluon field <sup>1</sup>

$$\mathcal{L}_{i=11-12} = \frac{C\alpha_s(2m_\chi)}{4\Lambda_i^3} (\bar{\chi}\Gamma\chi) G^{a\mu\nu} G_{\mu\nu}^a \quad (6)$$

$$\mathcal{L}_{i=13-14} = \frac{C\alpha_s(2m_\chi)}{4\Lambda_i^3} (\bar{\chi}\Gamma\chi) G^{a\mu\nu} \tilde{G}_{\mu\nu}^a \quad (7)$$

where  $\Gamma = 1$  or  $i\gamma^5$ . For operators involving gluons, the factor of strong coupling constant  $\alpha_s(2m_\chi)$  is also included in accord with the trace anomaly and is evaluated at the scale  $2m_\chi$  where  $m_\chi$  is the dark matter mass.

Finally, we also write down the corresponding operators for complex scalar dark matter. Again, we note that the interactions for real scalar dark matter is similar to complex one and differ by a factor of two. We simply focus on the complex scalar dark matter. The operators corresponding to vector boson exchange are

$$\mathcal{L}_{i=15,16} = \frac{C}{\Lambda_i^2} \left( \chi^\dagger \overleftrightarrow{\partial}_\mu \chi \right) (\bar{q}\gamma^\mu\Gamma q) , \quad (8)$$

where  $\Gamma = 1$  or  $\gamma^5$  and  $\chi^\dagger \overleftrightarrow{\partial}_\mu \chi = \chi^\dagger(\partial_\mu\chi) - (\partial_\mu\chi^\dagger)\chi$ . Those corresponding to a scalar boson exchange are

$$\mathcal{L}_{i=17,18} = \frac{Cm_q}{\Lambda_i^2} (\chi^\dagger\chi) (\bar{q}\Gamma q) , \quad (9)$$

---

<sup>1</sup> We do not study the other gauge bosons, like  $W$  and  $Z$  bosons, because they decay into light quarks which then fragment into photons, would be softer in this case.

where  $\Gamma = 1$  or  $i\gamma^5$ . The corresponding gluonic operators are

$$\mathcal{L}_{i=19} = \frac{C\alpha_s(2m_\chi)}{4\Lambda_i^3} (\chi^\dagger\chi) G^{a\mu\nu}G_{a\mu\nu} , \quad (10)$$

$$\mathcal{L}_{i=20} = \frac{iC\alpha_s(2m_\chi)}{4\Lambda_i^3} (\chi^\dagger\chi) G^{a\mu\nu}\tilde{G}_{a\mu\nu} . \quad (11)$$

The whole set of operators we are studying are tabulated in Table I together with their corresponding coefficients and scaling with velocities in the annihilation cross sections. Without a particular model in mind we will treat each interaction independently in our analysis by considering one operator at a time and setting the coefficient  $C = 1$  for simplicity.<sup>2</sup> The relative importance of each operator can be understood by considering the non-relativistic expansion of the operator and studying the velocity dependence. It was fully discussed in Ref. [13] and hence we only briefly summarize here for convenience. In the non-relativistic limit, the spinors for the Dirac DM  $\chi$  and  $\bar{\chi}$  annihilation are  $\psi \simeq (\xi, \epsilon\xi)^T$  and  $\bar{\psi} \simeq (\epsilon\eta^\dagger, \eta^\dagger)\gamma^0$  where  $\xi$  and  $\eta$  are two-components Pauli spinors and  $\epsilon = O(v/c)$ . We can expand  $\bar{\psi}\gamma^\mu\psi$  as

$$\begin{aligned} \bar{\psi}\gamma^0\psi &\simeq 2\epsilon\eta^\dagger\xi \\ \bar{\psi}\gamma^i\psi &\simeq (1 + \epsilon^2)\eta^\dagger\sigma_i\xi \end{aligned}$$

where the spatial components are not suppressed by  $v/c$ . On the other hand,  $\bar{\psi}\gamma^\mu\gamma^5\psi$  in the non-relativistic limit are

$$\begin{aligned} \bar{\psi}\gamma^0\gamma^5\psi &\simeq (1 + \epsilon^2)\eta^\dagger\xi \\ \bar{\psi}\gamma^i\gamma^5\psi &\simeq 2\epsilon\eta^\dagger\sigma_i\xi \end{aligned}$$

where the spatial components are now suppressed by  $v/c$ . It is clear that in the non-relativistic limit the time and spatial components of the vector and axial vector bilinear behave very differently. We can then consider them separately when it is contracted with the trace of the light quark leg. If we look at the trace of  $(\bar{q}\gamma^\mu q)$  or  $(\bar{q}\gamma^\mu\gamma^5 q)$  in the annihilation amplitude, the time component part after being squared gives a quantity close to zero, while the spatial component part gives a quantity in the order of  $m_\chi^2$ . Therefore, it is clear now that  $\bar{\psi}\gamma^\mu\psi$  multiplied to  $(\bar{q}\gamma_\mu q)$  or  $(\bar{q}\gamma_\mu\gamma^5 q)$  will not be suppressed, while  $\bar{\psi}\gamma^\mu\gamma^5\psi$  multiplied to  $(\bar{q}\gamma_\mu q)$  or  $(\bar{q}\gamma_\mu\gamma^5 q)$  will always be suppressed. Therefore, the operators  $O_1$  and  $O_3$  can contribute to annihilation much more than the operators  $O_2$  and  $O_4$ . Thus, the limits on

---

<sup>2</sup> For gluonic operators, their coefficients  $C$ s are induced at loop level and can be smaller.



$O_1$  and  $O_3$  are much stronger than  $O_2$  and  $O_4$ . All the other operators listed in Table I can be understood similarly [13]. We note that some of the operators are doubly suppressed by the velocity of the dark matter combined with either a light quark mass or strong coupling constant.

In the calculation of the gamma-ray flux from dark matter annihilation presented in the next section, we only include the light-quark flavors. We ignore the  $\chi\bar{\chi} \rightarrow t\bar{t}$  contribution, because the  $t$  and  $\bar{t}$  first decay into  $bW \rightarrow bq\bar{q}'$  before each light quark undergoes fragmentation into hadrons, including pions. Therefore, the gamma-ray spectrum would be significantly softer than the direct fragmentation as in  $\chi\bar{\chi} \rightarrow q\bar{q}$  [13].

Note that some of the lower limits that we obtain in Table III are relative low compared to the dark matter mass. Notably for the operators  $O_{7,9}$ ,  $O_{11,13}$ ,  $O_{15,16}$  and  $O_{17,18}$ . In such cases, one may question the validity of the effective interaction approach. The physics behind is easy to understand. The effects of such operators are very suppressed because of the small velocity suppression or helicity suppression, not because of the size of the  $\Lambda$ . Therefore, the  $\Lambda$  has to be small enough in order to see an effect from these operators. We argue that the effective momentum transfer of such velocity-suppressed operators should be  $m_\chi(v/c)$ . With  $(v/c) \sim 10^{-3}$  for the DM velocity at the present epoch, as long as the ratio  $m_\chi(v/c)/\Lambda$  remains small, we expect the effective interaction approach can still be valid.

### III. GAMMA-RAY FLUX

#### A. Background Diffuse Gamma Rays

The Galactic diffuse gamma rays originate primarily from the interactions of high energy charged particles contained in cosmic rays with the nuclei in the interstellar medium and the associated radiation fields of the charged particles, via a few of the following mechanisms.

- (i) Gamma-rays coming from the  $\pi^0$  decay, which in turn comes from the interactions of the cosmic rays with the nucleons in the interstellar medium. This dominates the background flux for energy higher than 1 GeV.
- (ii) Inverse Compton scattering occurs when high energy  $e^\pm$  collide with the photons of the interstellar medium.

- (iii) Bremsstrahlung photons occur when high energy  $e^\pm$  are deflected by the Coulomb field of the interstellar medium.
- (iv) Synchrotron radiation occurs when high energy  $e^\pm$  are deflected by Galactic magnetic field.
- (v) An extragalactic background, which is expected to be isotropic and receives contributions from many sources including unresolved point sources, diffuse emission from large scale structure formation and from interactions between ultra-high energy cosmic rays and relic photons, etc. This background is the least determined and so a fairly large uncertainty is associated with it. The Fermi-LAT has a measurement of diffuse gamma-ray in the mid-latitude region and fitted the extra-galactic background by

$$E^2 \frac{d\Phi}{dE} = A \left( \frac{E}{0.281 \text{ GeV}} \right)^\delta, \quad (12)$$

where  $A$  and  $\delta$  are fitted parameters (the power-law index is  $\gamma = |\delta - 2|$ ). In Ref. [19], the power-law is fitted to be  $\gamma = 2.41 \pm 0.05$  and  $A$  can be determined by the total flux of EGB (“extragalactic” diffuse gamma-ray emission) as  $A = (0.95^{+0.18}_{-0.17}) \times 10^{-6} \text{ GeV cm}^{-2} \text{ s}^{-1} \text{ sr}^{-1}$  for  $E > 100 \text{ MeV}$ .

Since Fermi-LAT did not give details about the parameters of GALPROP (Cosmic ray propagation code) [22] that they used in their treatment, we run GALPROP (the web version) to obtain the various diffuse Galactic backgrounds (i) to (iv) and fit EGB component in Eq. (12) to Fermi-LAT data. The relevant GALPROP parameters that we used are shown in Table II. Our fitted EGB is given by

$$E^2 \frac{d\Phi}{dE} = (0.99 \times 10^{-6}) \left( \frac{E}{0.281 \text{ GeV}} \right)^{-0.36} \text{ GeV cm}^{-2} \text{ s}^{-1} \text{ sr}^{-1} \quad (13)$$

which gives a power-law index  $\gamma = 2.36$  and  $E$  is in GeV. It is close enough to the one obtained by Fermi-LAT. The  $\chi^2 = 2.435$  for 7 d.o.f. The various curves are all within the uncertainties quoted in the Fig. 6(a) of the Fermi-LAT paper [19]. Various diffuse background curves and their sum are shown in Fig. 1.

## B. Dark Matter Annihilation

The dominant DM contribution to photon flux in this scenario comes from

$$\chi\bar{\chi} \rightarrow q\bar{q} \rightarrow \pi^0 + X \rightarrow 2\gamma + X, \quad (14)$$

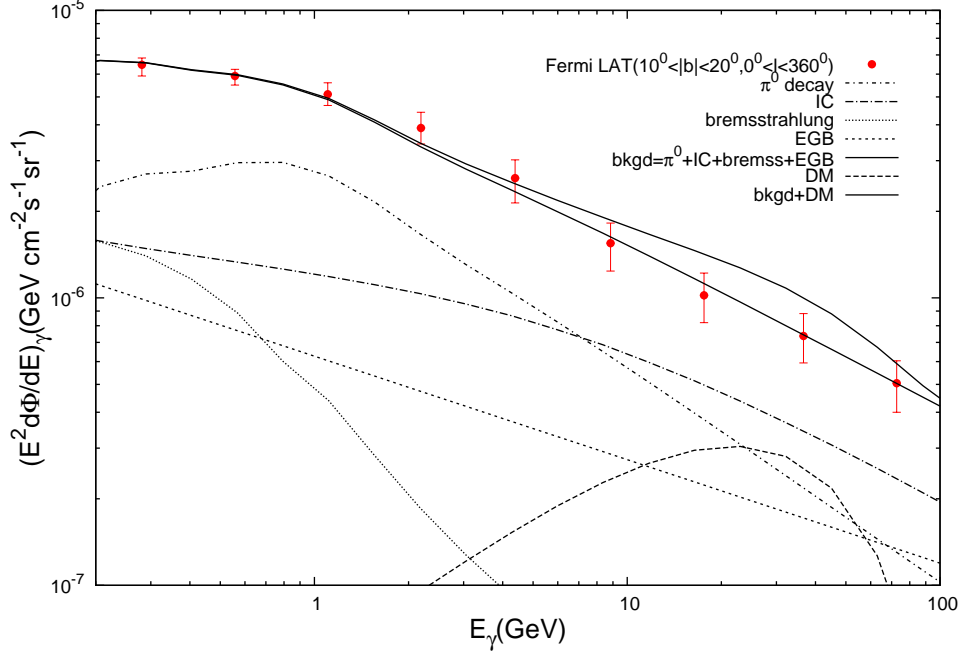


FIG. 1. The photon spectrum  $E^2(d\Phi/dE_\gamma)$  versus the photon energy for the diffuse background gamma rays, including  $\pi^0$  decays (short-dashed-dotted) from interactions of cosmic rays with interstellar medium, inverse Compton scattering IC (long-dashed-dotted), bremsstrahlung (dotted) and extragalactic EGB (short-dashed). Their sum is shown as the lower solid line. A dark matter component due to DM annihilation of  $\chi\bar{\chi} \rightarrow q\bar{q}$  is also shown (long-dashed) and added to the total background (upper solid line). The DM annihilation is due to a 200 GeV DM particle with the effective interaction operator  $O_1$  and  $\Lambda = 1.5$  TeV.

in which all the  $q, \bar{q}$  ( $q = u, d, c, s, b$ ) have probabilities fragmenting into  $\pi^0$ , which then decay almost entirely into two photons. As mentioned in the Introduction, we employ two approaches of obtaining the photon spectrum due to fragmentation of light quarks. (i) Using the process  $e^+e^- \rightarrow q\bar{q}$  with initial radiations turned off in Pythia [20] and extracting the photon spectrum in the final state. The photon mainly comes from the decay of  $\pi^0$ , which are in turn produced by fragmentation of light quarks, plus a very small fraction from the bremsstrahlung photon off the quark legs. (ii) Using the fragmentation function of  $q, \bar{q}, g$  into  $\pi^0$  from the fitting of Ref. [21], then convoluting with the  $dN/dE_\gamma(\pi^0 \rightarrow \gamma\gamma)$  to obtain the photon spectrum of quarks into photon. Both approaches give the photon spectra close enough to each other for our purpose of numerical calculations. Thus, the resulting limits using both approaches are also the same within numerical accuracy. However, we have

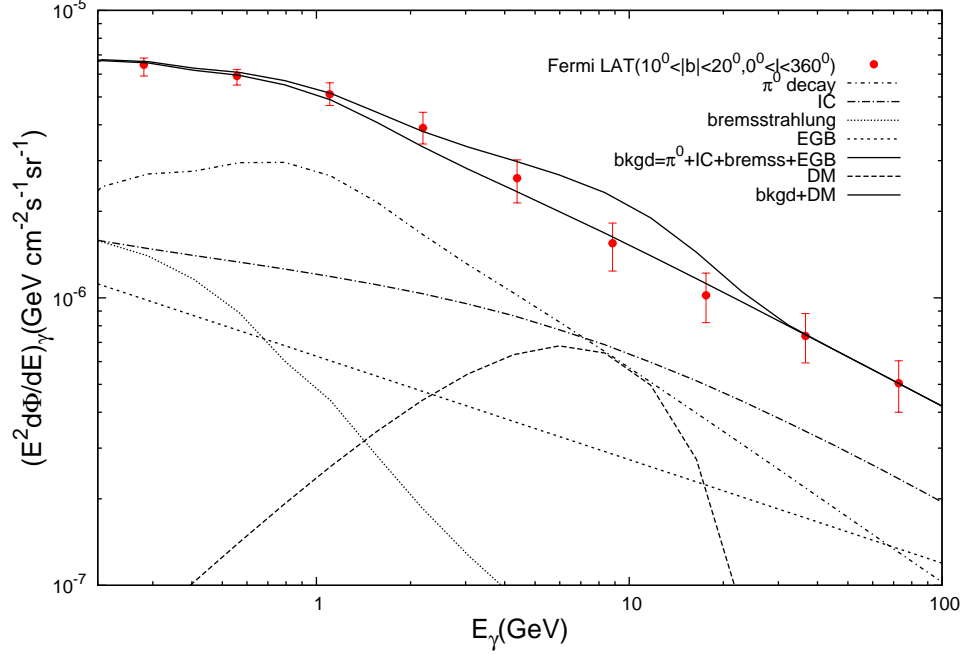


FIG. 2. Same as Fig. 1 but the DM annihilation is due to a 50 GeV dark matter particle with the effective interaction operator  $O_1$  and  $\Lambda = 0.87$  TeV.

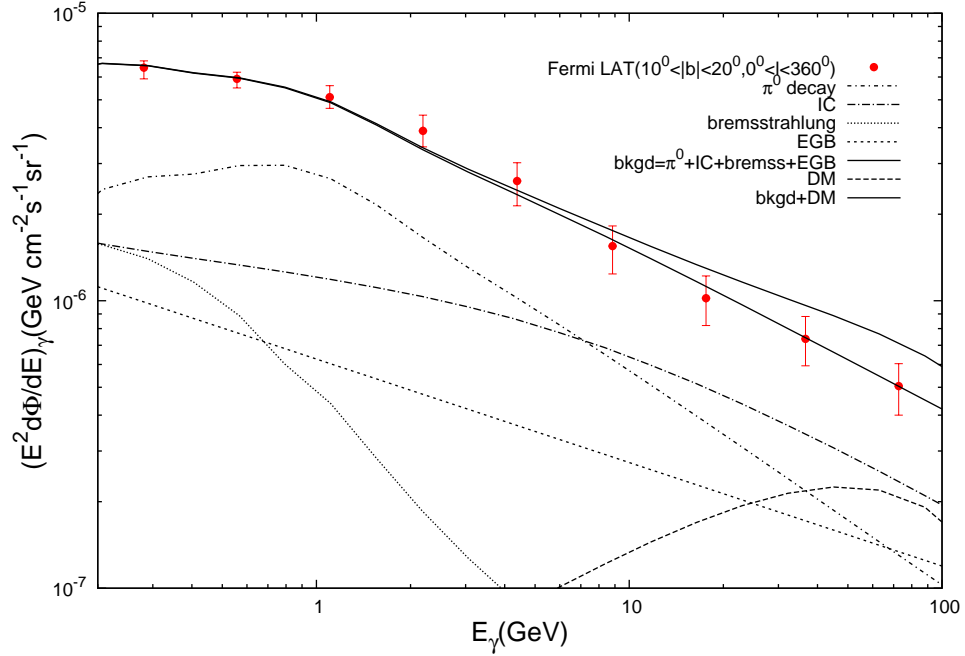


FIG. 3. Same as Fig. 1 but the DM annihilation is due to a 500 GeV dark matter particle with the effective interaction operator  $O_1$  and  $\Lambda = 1.9$  TeV.

to use the second approach when we place limits on the operators involving gluons in the annihilation, because we do not find a simple process in Pythia for extraction of  $g \rightarrow \gamma$

TABLE II. The values of the parameters that we used in running the code GALPROP to reproduce the background curves in Figs. 1–3. For unstated parameters we employ the default values.

Parameter (unit)	Value
Minimum galactocentric radius $r_{min}$ (kpc)	00.0
Maximum galactocentric radius $r_{max}$ (kpc)	25.0
Minimum height $z_{min}$ (kpc)	−04.0
Maximum height $z_{max}$ (kpc)	+04.0
ISRF factors for IC calculation: optical, FIR, CMB $ISRF_{factors}$	1.9, 1.9, 1.9
Gamma-ray Intensity Skymap Longitude minimum $long_{min}$ (degrees)	0.0
Gamma-ray Intensity Skymap Longitude maximum $long_{max}$ (degrees)	360.0
Gamma-ray Intensity Skymap Latitude minimum $lat_{min}$ (degrees)	+10.0
Gamma-ray Intensity Skymap Latitude maximum $lat_{max}$ (degrees)	+20.0
Binsize in Longitude for Gamma-ray Intensity Skymaps $d_{long}$ (degrees)	0.50
Binsize in Latitude for Gamma-ray Intensity Skymaps $d_{lat}$ (degrees)	0.50
Diffusion Coefficient Normalization $D_{0xx}$ ( $10^{28} \text{ cm}^2 \text{ s}^{-1}$ )	6.1
Diffusion Coefficient Index Below Break Rigidity $D_{g1}$	0.33
Diffusion Coefficient Index Above Break Rigidity $D_{g2}$	0.33
Diffusion Coefficient Break Rigidity $D_{rigid\ br}$ ( $10^3 \text{ MV}$ )	4.0
Alfven Speed $v_A$ ( $\text{km s}^{-1}$ )	30
Nuclear Break Rigidity $nuc_{rigid\ br}$ ( $10^3 \text{ MV}$ )	10.0
Nucleus Injection Index Below Break Rigidity $nuc_{g1}$	2.00
Nucleus Injection Index Above Break Rigidity $nuc_{g2}$	2.43
Proton Flux Normalization ( $10^{-9} \text{ cm}^{-2} \text{ sr}^{-1} \text{ s}^{-1} \text{ MeV}^{-1}$ )	4.90
Proton Kinetic Energy for Normalization ( $10^5 \text{ MeV}$ )	1.00
Electron Break Rigidity0 $electron_{rigid\ br0}$ ( $10^4 \text{ MV}$ )	3.0
Electron Break Rigidity $electron_{rigid\ br}$ ( $10^9 \text{ MV}$ )	1.0
Electron Injection Index Below Break Rigidity0 $electron_{g0}$	2.20
Electron Injection Index Above Break Rigidity0 and Below Break Rigidity $electron_{g1}$	2.54
Electron Injection Index Above Break Rigidity $electron_{g2}$	2.5
Electron Flux Normalization ( $10^{-10} \text{ cm}^{-2} \text{ sr}^{-1} \text{ s}^{-1} \text{ MeV}^{-1}$ )	4.0
Electron Kinetic Energy for Normalization ( $10^4 \text{ MeV}$ )	3.45

fragmentation.

The photon flux is proportional to the square of the number density of the DM particles  $(\rho/m_\chi)^2$ , the annihilation cross section  $\langle\sigma v\rangle$  and the spectrum of photons  $dN/dE_\gamma$  per annihilation. The flux observed is found by integrating the number density squared along the line-of-sight connecting from the source to the observer, given by

$$\Phi = \frac{\langle\sigma v\rangle}{2} \frac{dN}{dE_\gamma} \frac{1}{4\pi m_\chi^2} \int_{\text{line of sight}} ds \rho^2(s, \psi) , \quad (15)$$

where  $s$  runs along the line of sight and  $\psi$  is the angle from the direction of the Galactic Center. Here the factor of 2 in the denominator accounts for particle-antiparticle annihilation since we are dealing with Dirac or complex scalar DM. We employ the isothermal profile in running the GALPROP [22].

The contribution from annihilation of DM to the observed diffuse photon spectrum is shown in each Fig. 1 – Fig. 3 (the long dashed curve near the bottom of each figure.) The position of the peak of the DM curve corresponds to about  $0.1m_\chi$ , as can be clearly spotted at each of these figures. When we add the DM contribution to the total background curve, we see the deviation from the data points. We can quantify the deviation from the data by calculating the total  $\chi^2$  as a function of DM mass and the interaction strength of the annihilation (given by  $\Lambda^2$ ).

Here we adopt a simple statistical measure to quantify the effect of each operator. We calculate the  $3\sigma$  limit on each scale  $\Lambda_i$ . We assume the data agree well with the expected background, and then we calculate the  $\chi^2$  with finite  $\Lambda_i$ 's until we obtain a  $\chi^2$  difference of  $\Delta\chi^2 \equiv \chi^2 - \chi_{\text{bkgd}}^2 = 9$  ( $3\sigma$ ). The DM curve in each figure corresponds to a  $3\sigma$  deviation from the data points. We calculate the limit for each operator and list them in Table III. For those unsuppressed operators the limit is of order 1 TeV for  $m_\chi = 50 - 500$  GeV. But for those operators suppressed by the velocity of the DM, light quark masses or strong coupling constant, the limit is significantly weaker of order 0.01 – 0.1 TeV.

Once we obtained the lower limits on  $\Lambda$  for each DM mass, we can calculate the corresponding upper limits on  $\langle\sigma v\rangle(\chi\bar{\chi} \rightarrow q\bar{q})$  as a function of DM mass. We found that these upper limits on  $\langle\sigma v\rangle(\chi\bar{\chi} \rightarrow q\bar{q})$  are approximately independent of the operators with  $q$  and  $\bar{q}$  in the final state. We understand this as the fragmentation process of  $q$  or  $\bar{q}$  into  $\pi^0$  followed by  $\pi^0 \rightarrow \gamma\gamma$  decays does not depend on how the quarks are produced. As long as the quarks produced have the same energy, the fragmentation rate or pattern should be the

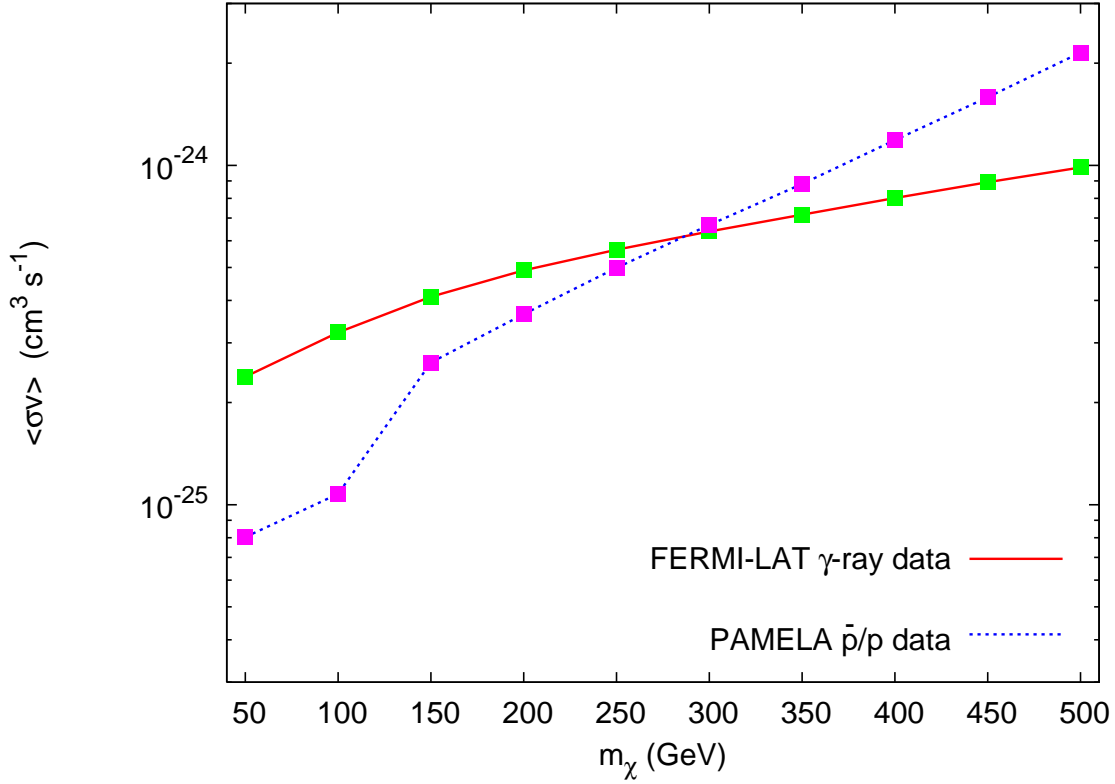


FIG. 4. The  $3\sigma$  upper limits on the annihilation cross section  $\sigma v(\chi\bar{\chi} \rightarrow q\bar{q})$  versus the DM mass due to the Fermi-LAT photon-flux data ( $10^\circ < |b| < 20^\circ$ ,  $0^\circ < l < 360^\circ$ ) and due to the PAMELA antiproton-flux data [13]. The limits are approximately independent of the operators. The annihilation cross sections above the curves are ruled out. The  $x$ -axis is at the value  $3 \times 10^{-26} \text{cm}^3 \text{s}^{-1}$  which is the required annihilation cross section to give the correct thermal relic density.

same. We show in Fig. 4 the upper limits on  $\langle\sigma v\rangle(\chi\bar{\chi} \rightarrow q\bar{q})$  allowed by the Fermi-LAT photon-flux data, as well as those obtained in Ref. [13] using the antiproton-flux data of PAMELA [23]. It is clear in Fig. 4 that the antiproton-flux data from PAMELA does give a stronger constraint on the annihilation cross section  $\langle\sigma v\rangle(\chi\bar{\chi} \rightarrow q\bar{q})$  than the Fermi-LAT photon-flux data for lighter DM (50 – 300 GeV), while Fermi-LAT gamma-ray data does constrain stronger for heavier DM mass (300 – 500 GeV).

TABLE III. The  $3\sigma$  lower limits on the effective scale  $\Lambda$  of each operator listed in Table I. We take the coefficient  $C = 1$  with  $m_\chi = 50, 100, 200$  and  $500$  GeV.

Operators	$\Lambda$ (TeV)			
	$m_\chi$ (GeV) = 50	100	200	500
Dirac DM, (axial) vector/tensor exchange				
$O_1 = (\bar{\chi}\gamma^\mu\chi)(\bar{q}\gamma_\mu q)$	0.87	1.15	1.46	1.94
$O_2 = (\bar{\chi}\gamma^\mu\gamma^5\chi)(\bar{q}\gamma_\mu q)$	0.025	0.033	0.042	0.055
$O_3 = (\bar{\chi}\gamma^\mu\chi)(\bar{q}\gamma_\mu\gamma^5 q)$	0.87	1.15	1.46	1.94
$O_4 = (\bar{\chi}\gamma^\mu\gamma^5\chi)(\bar{q}\gamma_\mu\gamma^5 q)$	0.13	0.12	0.11	0.10
$O_5 = (\bar{\chi}\sigma^{\mu\nu}\chi)(\bar{q}\sigma_{\mu\nu} q)$	1.04	1.36	1.74	2.31
$O_6 = (\bar{\chi}\sigma^{\mu\nu}\gamma^5\chi)(\bar{q}\sigma_{\mu\nu} q)$	1.04	1.36	1.74	2.31
Dirac DM, (pseudo) scalar exchange				
$O_7 = (\bar{\chi}\chi)(\bar{q}q)$	0.009	0.011	0.014	0.017
$O_8 = (\bar{\chi}\gamma^5\chi)(\bar{q}q)$	0.094	0.11	0.14	0.17
$O_9 = (\bar{\chi}\chi)(\bar{q}\gamma^5 q)$	0.009	0.011	0.014	0.017
$O_{10} = (\bar{\chi}\gamma^5\chi)(\bar{q}\gamma^5 q)$	0.094	0.11	0.14	0.17
Dirac DM, gluonic				
$O_{11} = (\bar{\chi}\chi)G_{\mu\nu}G^{\mu\nu}$	0.011	0.013	0.017	0.024
$O_{12} = (\bar{\chi}\gamma^5\chi)G_{\mu\nu}G^{\mu\nu}$	0.11	0.13	0.17	0.24
$O_{13} = (\bar{\chi}\chi)G_{\mu\nu}\tilde{G}^{\mu\nu}$	0.011	0.013	0.017	0.024
$O_{14} = (\bar{\chi}\gamma^5\chi)G_{\mu\nu}\tilde{G}^{\mu\nu}$	0.11	0.13	0.17	0.24
Complex Scalar DM, (axial) vector exchange				
$O_{15} = (\chi^\dagger \overleftrightarrow{\partial}_\mu \chi)(\bar{q}\gamma^\mu q)$	0.025	0.033	0.042	0.055
$O_{16} = (\chi^\dagger \overleftrightarrow{\partial}_\mu \chi)(\bar{q}\gamma^\mu\gamma^5 q)$	0.025	0.033	0.042	0.055
Complex Scalar DM, (pseudo) scalar exchange				
$O_{17} = (\chi^\dagger \chi)(\bar{q}q)$	0.11	0.10	0.095	0.083
$O_{18} = (\chi^\dagger \chi)(\bar{q}\gamma^5 q)$	0.11	0.10	0.095	0.083
Complex Scalar DM, gluonic				
$O_{19} = (\chi^\dagger \chi)G_{\mu\nu}G^{\mu\nu}$	0.13	0.13	0.13	0.14
$O_{20} = (\chi^\dagger \chi)G_{\mu\nu}\tilde{G}^{\mu\nu}$	0.13	0.13	0.13	0.14



## IV. DISCUSSION AND CONCLUSIONS

Here we do a comparison with the limits obtained in collider [3–5], gamma-ray lines in Ref. [8], antiproton flux [13] and direct searches.

- *Comparison to limits obtained using gamma-ray lines [8] against the Fermi-LAT data [19].* As mentioned before, our continuum gamma-ray signals are obtained via quark or antiquark fragmentation, whereas in Ref. [8] the discrete gamma-ray line is coming from one-loop dressing of the effective operators. Note also that we are calculating the  $3\sigma$  lower limit while Ref. [8] reported the 95% C.L. lower limits, which are approximately  $2\sigma$ , so our limits are slightly more conservative. We found that the limits for operator  $O_{1,3}$  are substantially better than the corresponding operators  $D_{5,7}$  of Ref. [8]. Our limits are 0.9–1.9 TeV for  $m_\chi = 50$ –500 GeV, while their limits are 0.12–0.6 TeV for  $m_\chi = 50$ –200 GeV. We see in this case (Dirac DM with vector-boson exchange), the contribution to photon flux through the continuum ( $q \rightarrow \pi^0 \rightarrow \gamma$ ) is substantially better than the discrete line spectrum (via the loop process) when compared against the Fermi-LAT data. The limits for operators  $O_{7-10}$  (Dirac DM with scalar-boson exchange) and  $O_{17,18}$  (complex scalar DM with scalar-boson exchange) are about the same as  $D_{1-4}$  and  $C_{1,2}$ , respectively, of Ref. [8]. On the other hand, limits for operators  $O_{15,16}$  (complex scalar DM with vector-boson exchange) are weaker than  $C_{3,4}$  of Ref. [8].
- *Comparison to limits obtained using antiproton flux [13] against the PAMELA antiproton data [23].* The approach that we did in Ref. [13] is very similar to the work here, except that we require to see photon instead of antiproton in the final state and we are comparing with two entirely different categories of data. We found that at the lower end  $m_\chi \sim 50$ –300 GeV the limits from antiproton data are somewhat better than those from photon-flux data. This is because of the nature of the fragmentation and decay chain: one fragments into antiproton directly while the other one fragments into  $\pi^0$  then followed by decays of  $\pi^0 \rightarrow \gamma\gamma$ . The peak of the antiproton spectrum occurs at larger energies than the peak of the photon spectrum for the same DM mass. On the other hand, when  $m_\chi$  increases to about 300–500 GeV, limits from gamma-ray flux constrains stronger on the DM interactions.

- *Comparison to limits obtained using collider data* [4, 5]. The collider limits on  $\Lambda$  come from monojet plus missing energy data. Basically, for operators that are velocity suppressed, e.g.,  $O_{2,4}$  among  $O_{1-4}$ , the limits from photon flux are not as good as those from colliders; and vice versa for operators that are not velocity suppressed, e.g.,  $O_{1,3}$  among  $O_{1-4}$ . The collider limits for  $O_{1-4}$  are  $200 - 300$  GeV, while the limits from photon flux are  $0.9 - 1.9$  TeV for  $O_{1,3}$  but only  $25 - 100$  GeV for  $O_{2,4}$ . The operators for which photon flux gives better limits are  $O_{1,3}$ ,  $O_{5,6}$ ,  $O_{8,10}$ ,  $O_{12,14}$ ,  $O_{17,18}$  and  $O_{19,20}$ .
- *Comparison to limits obtained by the direct detection experiments* [24, 25]. Two most stringent experiments on the spin-independent (SI) cross sections come from CDMS [24] and XENON100 [25]. The best upper limit from CDMS [24] is  $\sigma_{\chi N}^{\text{SI}} \simeq 3.8 \times 10^{-44} \text{ cm}^2$  at  $m_\chi = 70$  GeV and from XENON100 [25] is  $\sigma_{\chi N}^{\text{SI}} \simeq 0.7 \times 10^{-44}$  at  $m_\chi = 50$  GeV. Note that only the operators  $O_1$  and  $O_7$  for Dirac DM contribute to spin-independent cross sections. For  $O_7 = m_q(\bar{\chi}\chi)(\bar{q}q)/\Lambda_7^3$  the SI cross section is given by

$$\sigma_{\chi N}^{\text{SI}} = \frac{\mu_{\chi N}^2}{\pi} |G_s^N|^2, \quad (16)$$

where  $\mu_{\chi N}$  is the reduced mass of the DM and nucleon, and

$$G_s^N = \sum_q \langle N | \bar{q}q | N \rangle \left( \frac{m_q}{\Lambda^3} \right), \quad \langle N | \bar{q}q | N \rangle = \frac{m_N}{m_q} \times \begin{cases} f_{Tq}^N & : \text{ light quarks} \\ \frac{2}{27} f_{Tg}^N & : \text{ heavy quarks} \end{cases}. \quad (17)$$

Using the default values of  $f_{Tq}^N$  and  $f_{Tg}^N$  adopted in DarkSUSY [26] and averaging between the neutron and proton for  $\sigma_{\chi N}^{\text{SI}}$ , we obtain

$$\sigma_{\chi N}^{\text{SI}} \simeq \frac{m_N^4}{\pi \Lambda_7^6} (0.3769)^2. \quad (18)$$

Using the limit  $\sigma_{\chi N}^{\text{SI}} < 10^{-44} \text{ cm}^2$  for  $m_\chi \sim 50 - 200$  GeV [25], we obtain

$$\Lambda_7 > 330 \text{ GeV}. \quad (19)$$

This limit is much better than the limit on  $O_7$  shown in Table III. On the other hand, with the operator  $O_1 = (\bar{\chi}\gamma^\mu\chi)(\bar{q}\gamma_\mu q)/\Lambda_1^2$  we obtain

$$\sigma_{\chi N}^{\text{SI}} = \frac{\mu_{\chi N}^2}{256\pi} |b_N|^2, \quad (20)$$

where  $b_N \simeq \frac{3}{2}(\alpha_u^V + \alpha_d^V)$ , which is obtained by taking the average of neutrons and protons inside a nucleon, and  $\alpha_{u,d}^V = 1/\Lambda_1^2$  are the coefficients in front of the operators for the valence  $u$  and  $d$  quark. We therefore obtain

$$\sigma_{\chi N}^{\text{SI}} \simeq \frac{9}{256\pi} \frac{m_N^2}{\Lambda_1^4}, \quad (21)$$

which gives the limit on  $\Lambda_1$ , with  $\sigma_{\chi N}^{\text{SI}} < 10^{-44} \text{ cm}^2$ , as

$$\Lambda_1 > 4.4 \text{ TeV}. \quad (22)$$

It is about 2 – 3 times better than the corresponding limits on  $O_1$  shown in Table III.

In summary, we have used an effective interaction approach to investigate the effects of dark matter interactions with light quarks on diffuse photon flux coming from the mid-latitude ( $10^\circ < |b| < 20^\circ$ ,  $0^\circ < l < 360^\circ$ ) region. We have assumed a standard halo density while using the GALPROP to calculate the resulting diffuse gamma-ray spectrum. The diffuse gamma-ray background includes  $\pi^0$  decays produced by scattering of cosmic rays with the interstellar medium, inverse Compton scattering, bremsstrahlung, synchrotron radiation and extragalactic diffuse gamma rays. The background can reproduce the data recorded by Fermi-LAT very well. Dark matter annihilation provides yet another source of diffuse gamma rays. The dominant mechanism is annihilation into light quarks, followed by fragmentation into neutral pions, which then further decay into photons. The gamma-ray spectrum has no particular feature but a continuum; nevertheless, the flux is large. We have shown that the effective interactions of the DM can give rise to a nontrivial contribution to the diffuse gamma-ray spectrum, as presented in various figures.

We have successfully used the data to obtain  $3\sigma$  limits on the scale  $\Lambda_i$ . The best limits are from the Dirac DM with vector or tensor boson exchanges. The limits for  $O_{1,3}$  and  $O_{5,6}$  are about 1 – 2 TeV, while other operators suppressed either by the velocity of dark matter, light quark masses or strong coupling constant give milder limits. Note that these limits from photon flux are *lower* limits on  $\Lambda_i$ . We found that the limits obtained are very comparable to those obtained using collider [4, 5], gamma-ray line search [8] and anti-matter experiments [13]. However, the two operators  $(\bar{\chi}\chi)(\bar{q}q)$  and  $(\bar{\chi}\gamma^\mu\chi)(\bar{q}\gamma_\mu q)$ , which contribute to spin-independent cross sections, are constrained more severely by the recent XENON100 data.

## ACKNOWLEDGMENTS

This work was supported in parts by the National Science Council of Taiwan under Grant Nos. 99-2112-M-007-005-MY3 and 98-2112-M-001-014-MY3 as well as the WCU program through the KOSEF funded by the MEST (R31-2008-000-10057-0).

---

- [1] E. Komatsu *et al.* [WMAP Collaboration], “Seven-Year Wilkinson Microwave Anisotropy Probe (WMAP) Observations: Cosmological Interpretation,” *Astrophys. J. Suppl.* **192**, 18 (2011) [arXiv:1001.4538 [astro-ph.CO]].
- [2] G. Bertone, D. Hooper and J. Silk, “Particle dark matter: Evidence, candidates and constraints,” *Phys. Rept.* **405**, 279 (2005) [arXiv:hep-ph/0404175].
- [3] Q. H. Cao, C. R. Chen, C. S. Li and H. Zhang, “Effective Dark Matter Model: Relic density, CDMS II, Fermi LAT and LHC,” arXiv:0912.4511 [hep-ph].
- [4] Y. Bai, P. J. Fox and R. Harnik, “The Tevatron at the Frontier of Dark Matter Direct Detection,” arXiv:1005.3797 [hep-ph].
- [5] J. Goodman, M. Ibe, A. Rajaraman, W. Shepherd, T. M. P. Tait and H. -B. Yu, “Constraints on Dark Matter from Colliders,” *Phys. Rev.* **D82**, 116010 (2010) [arXiv:1008.1783 [hep-ph]].
- [6] M. Beltran, D. Hooper, E. W. Kolb, Z. A. C. Krusberg and T. M. P. Tait, “Maverick dark matter at colliders,” *JHEP* **1009**, 037 (2010) [arXiv:1002.4137 [hep-ph]].
- [7] G. D. Mack, T. D. Jacques, J. F. Beacom, N. F. Bell and H. Yuksel, “Conservative Constraints on Dark Matter Annihilation into Gamma Rays,” *Phys. Rev. D* **78**, 063542 (2008) [arXiv:0803.0157 [astro-ph]].
- [8] J. Goodman, M. Ibe, A. Rajaraman, W. Shepherd, T. M. P. Tait and H. B. P. Yu, “Gamma Ray Line Constraints on Effective Theories of Dark Matter,” arXiv:1009.0008 [hep-ph].
- [9] D. T. Cumberbatch, Y. L. Tsai and L. Roszkowski, “The impact of propagation uncertainties on the potential Dark Matter contribution to the Fermi LAT mid-latitude gamma-ray data,” *Phys. Rev. D* **82**, 103521 (2010) [arXiv:1003.2808 [astro-ph.HE]].
- [10] D. Hooper and L. Goodenough, “Dark Matter Annihilation in The Galactic Center As Seen by the Fermi Gamma Ray Space Telescope,” *Phys. Lett. B* **697**, 412 (2011) [arXiv:1010.2752 [hep-ph]].

- [11] J. Fan, M. Reece and L. T. Wang, “Non-relativistic effective theory of dark matter direct detection,” arXiv:1008.1591 [hep-ph].
- [12] K. Cheung, K. Mawatari, E. Senaha, P. Y. Tseng and T. C. Yuan, “The Top Window for Dark Matter,” JHEP **1010**, 081 (2010) [arXiv:1009.0618 [hep-ph]].
- [13] K. Cheung, P. Y. Tseng and T. C. Yuan, “Cosmic Antiproton Constraints on Effective Interactions of the Dark Matter,” JCAP **1101**, 004 (2011) [arXiv:1011.2310 [hep-ph]].
- [14] C. Boehm, T. Delahaye, P. Salati, F. Staub and R. K. Singh, “Implication of the PAMELA antiproton data for dark matter indirect detection at LHC,” JCAP **1006**, 013 (2010) [arXiv:0907.4511 [hep-ph]].
- [15] K. Cheung, J. Song and P. Y. Tseng, “Cosmic positron and antiproton constraints on the gauge-Higgs Dark Matter,” JCAP **1009**, 023 (2010) [arXiv:1007.0282 [hep-ph]].
- [16] P. Ciafaloni, M. Cirelli, D. Comelli, A. De Simone, A. Riotto and A. Urbano, “On the Importance of Electroweak Corrections for Majorana Dark Matter Indirect Detection,” arXiv:1104.2996 [hep-ph]; P. Ciafaloni, D. Comelli, A. Riotto, F. Sala, A. Strumia and A. Urbano, “Weak Corrections are Relevant for Dark Matter Indirect Detection,” JCAP **1103**, 019 (2011) [arXiv:1009.0224 [hep-ph]].
- [17] N. F. Bell, J. B. Dent, A. J. Galea, T. D. Jacques, L. M. Krauss and T. J. Weiler, “W/Z Bremsstrahlung as the Dominant Annihilation Channel for Dark Matter, Revisited,” arXiv:1104.3823 [hep-ph].
- [18] K. Nakamura *et al.* (Particle Data Group), J. Phys. **G37**, 075021 (2010).
- [19] A. A. Abdo *et al.* [The Fermi-LAT Collaboration], “The Spectrum of the Isotropic Diffuse Gamma-Ray Emission Derived From First-Year Fermi Large Area Telescope Data,” Phys. Rev. Lett. **104**, 101101 (2010) [arXiv:1002.3603 [astro-ph.HE]].
- [20] T. Sjostrand, S. Mrenna and P. Z. Skands, “A Brief Introduction to PYTHIA 8.1,” Comput. Phys. Commun. **178**, 852-867 (2008) [arXiv:0710.3820 [hep-ph]].
- [21] S. Albino, B. A. Kniehl and G. Kramer, “Fragmentation functions for light charged hadrons with complete quark flavour separation,” Nucl. Phys. B **725**, 181 (2005) [arXiv:hep-ph/0502188].
- [22] A. W. Strong, I. V. Moskalenko, T. A. Porter, G. Johannesson, E. Orlando and S. W. Digel, “The GALPROP Cosmic-Ray Propagation Code,” arXiv:0907.0559 [astro-ph.HE].

- [23] O. Adriani *et al.* [PAMELA Collaboration], “PAMELA results on the cosmic-ray antiproton flux from 60 MeV to 180 GeV in kinetic energy,” *Phys. Rev. Lett.* **105**, 121101 (2010) [arXiv:1007.0821 [astro-ph.HE]].
- [24] Z. Ahmed *et al.* [The CDMS-II Collaboration], *Science* **327**, 1619-1621 (2010). [arXiv:0912.3592 [astro-ph.CO]].
- [25] E. Aprile *et al.* [XENON100 Collaboration], arXiv:1104.2549 [astro-ph.CO].
- [26] P. Gondolo, J. Edsjo, P. Ullio, L. Bergstrom, M. Schelke and E. A. Baltz, *JCAP* 0407, 008 (2004) [arXiv:astro-ph/0406204].